

Flexural ductility of reinforced HSC beams strengthened with CFRP sheets

Seyed Hamid Hashemi[†]

Faculty of Engineering, Arak University, Shariati St., Farmandari Sq., Arak, P. O. Box 38139, Iran

Ali Akbar Maghsoudi[‡] and Reza Rahgozar^{‡†}

Civil Engineering Department, Kerman University, Kerman, Iran

(Received September 12, 2006, Accepted September 10, 2008)

Abstract. Externally bonding fiber reinforced polymer (FRP) sheets with an epoxy resin is an effective technique for strengthening and repairing reinforced concrete (RC) beams under flexural loads. Their resistance to electro-chemical corrosion, high strength-to-weight ratio, larger creep strain, fatigue resistance, and nonmagnetic and nonmetallic properties make carbon fiber reinforced polymer (CFRP) composites a viable alternative to bonding of steel plates in repair and rehabilitation of RC structures. The objective of this investigation is to study the effectiveness of CFRP sheets on ductility and flexural strength of reinforced high strength concrete (HSC) beams. This objective is achieved by conducting the following tasks: (1) flexural four-point testing of reinforced HSC beams strengthened with different amounts of cross-ply of CFRP sheets with different amount of tensile reinforcement up to failure; (2) calculating the effect of different layouts of CFRP sheets on the flexural strength; (3) Evaluating the failure modes; (4) developing an analytical procedure based on compatibility of deformations and equilibrium of forces to calculate the flexural strength of reinforced HSC beams strengthened with CFRP composites; and (5) comparing the analytical calculations with experimental results.

Keywords: CFRP; beams; high strength concrete; ductility; tensile bars.

1. Introduction

The technique of bonding steel plates using epoxy adhesives is recognized as an effective and convenient method for repair and rehabilitation of RC structures; however, the problems associated with the steel corrosion, handling due to excessive size and weight, undesirable formation of welds, partial composite action with the surface concrete, and debonding lead to the need for alternative materials and further research in this field. The high strength-to-weight ratio, resistance to electro-chemical corrosion, larger creep strain, good fatigue strength, potential for decreased installation

[†] Assistant Professor, E-mail: hamidhashemi55@yahoo.com

[‡] Assistant Professor, Corresponding author, E-mail: maghsoudi.a.a@mail.uk.ac.ir

^{‡†} Assistant Professor, E-mail: Rahgozar.r@mail.uk.ac.ir

costs and repairs due to lower weight in comparison with steel, and nonmagnetic and nonmetallic properties of carbon fiber reinforced polymer (CFRP) composites offer a viable alternative to bonding of steel plates. The emergence of high strength epoxies has also enhanced the feasibility of using CFRP sheets and carbon fiber fabric for repair and rehabilitation.

The flexural capacity of both prestressed and nonprestressed members may be increased through the external bonding of CFRP sheets and carbon fiber fabric. With the recent advancement in concrete technology and the availability of various types of mineral and chemical admixtures and very powerful superplasticizers, concrete with a compressive strength of up to 100 MPa can now be produced commercially with an acceptable level of variability using ordinary aggregates (FIP/CEB 1990). These developments have led to increased applications of high-strength concrete (HSC) all around the globe. The definition of HSC varies geographically and with time, depending mainly on the availability of raw materials and technical know-how and the demand from the construction industry. What was considered high-strength in the 1950s would now be classified as low-or at most medium-strength. In North American practice, concrete with a 28-day cylinder compressive strength of at least 41 MPa is regarded as HSC (ACI 1992). On the other hand, the FIP/CEB (1990) state-of-the-art report on HSC defines it as a concrete having a minimum 28-day compressive strength of 60 MPa. In the Southeast Asian region, concrete with a compressive strength as high as 80 MPa has been produced commercially for use in some high-rise buildings, including the Petronas Tower, the tallest building in the world. HSC offers many advantages over conventional concrete.

The high compressive strength can be used advantageously in compression members such as columns and piles. In columns, the reduction in size will lead to reduced dead load and subsequently to reduced total load on the foundation system. Smaller column size also means more available floor space. HSC can also be effectively used in structures such as plates, shells, and arches where high in-plane compression exists. The relatively higher compressive strength per unit volume and per unit weight will also significantly reduce the dead load of flexural members.

In addition, HSC possessing a highly dense microstructure is likely to enhance long-term durability of the structure. When the strength of concrete gets higher, some of its characteristics and engineering properties become different from those of normal-strength concrete (NSC) (Carrasquillo *et al.* 1981, FIP/CEB 1990, ACI 1992, Burg and Ost 1992, Mansur *et al.* 1994). These differences in material properties may have important consequences in terms of the structural behavior and design of HSC members. The design provisions contained in the major building codes are, in reality, based on tests conducted on NSC. While designing a structure using HSC, the designer—particularly in the Southeast Asian region—usually ignores the enhanced properties of concrete and possible changes in the overall response of the structure because of lack of adequate code guidance (Rashid *et al.* 2002). Earlier research concluded that although the tensile strength and fracture energy increase with an increase in compressive strength, High Strength Concrete is less ductile than normal concrete in both tension and compression.

1.1 Literature review

An *et al.* (1991) and Malek *et al.* (1998) presented analytical procedures to calculate the flexural strength of RC beams bonded with FRP plates. Concrete beams strengthened with externally bonded FRP strips were analyzed using the closed-form higher-order solutions by Rabinovitch *et al.* (2000). The strength of concrete beams bonded with CFRP sheets (Spadea *et al.* 1998, Grace *et al.* 1999), and GFRP plates (Saadatmanesh and Ehsani 1991) were studied experimentally.

The failure modes of concrete beams retrofitted with FRP materials and the techniques used in analyzing the failure modes were reviewed by Buyukozturk *et al.* (1998). The behavior of concrete beams strengthened with externally bonded FRP plates (Sharif *et al.* 1994, Mukhopadhyaya *et al.* 1998, Ross *et al.* 1999) and carbon fiber fabric (GangaRao *et al.* 1998) was studied both experimentally and analytically. Guidelines were presented by Sonobe *et al.* (1997) for the design of RC building structures using FRP composites. To date, extensive research work has been conducted on the flexural strength of concrete beams bonded with various types of FRP composites. Past research concluded applying FRP to the tensile face of a RC beam increases the stiffness and load capacity and decrease the deflection of RC beams. Advances in concrete technology in many countries have now made practical use of concrete with strengths up to 90 MPa. These concretes, with very high compressive strength, can result in less ductile responses of structural members. It has been found that flexural ductility, in terms of maximum curvatures attainable, may be smaller in HSC beams (ACI Committee 363 1992).

In seismic areas, ductility is an important factor in design of HSC members under flexure, consequently the use of HSC beams strengthened with CFRP and ductility that has not been focus in much of the previous experimental research will focus in this study.

Although external strengthening of RC beams using epoxy-bonded FRP has been established as an effective tool for increasing their flexural and/or shear strength, the method still suffers from some drawbacks. Many of these drawbacks are attributed to the characteristics of currently available commercial FRP strengthening systems. Although FRPs have high strengths, they are very brittle. When loaded in tension, FRPs exhibit a linear stress-strain behavior up to failure without exhibiting a yield plateau or any indication of an impending failure. The objective of this investigation is to study the effectiveness of CFRP sheets on ductility and flexural strength of high strength reinforced concrete beams. This objective is achieved by conducting the following tasks: (1) flexural testing of reinforced HSC beams strengthened with different amounts of cross-ply of CFRP sheets with different amount of tensile reinforcement ; (2) calculating the effect of different layouts of CFRP sheets on the flexural strength; (3) Evaluating the failure modes; (4) developing an analytical procedure to calculate the flexural strength of reinforced HSC beams strengthened with CFRP composites; and (5) comparing the analytical calculations with experimental results.

2. Reinforced hsc test beam details

Four-point bending flexural tests were conducted up to failure on two HSRC control beams and six HSRC beams strengthened with externally bonded FRP sheets on the tension face. The length, width, and depth ($L \times b \times h$) of all beams were kept as $3000 \times 150 \times 250$ mm. Each concrete beam was reinforced with two 16-mm diameter for A series and two 22-mm diameter for B series steel bars for tension and two 10-mm-diameter steel bars for compression along with 10-mm-diameter bars at a spacing of 90 mm center-to-center for shear reinforcement. The spacing of stirrups and maximum and minimum reinforcement ratios are in accordance with the provision of the American Concrete Institute (ACI). Electrical resistance disposable strain gauges, manufactured by TML Measurements Group (Japan), were pasted on the CFRP sheets and on internal reinforcing bars at different locations. The demec and electrical gauges were also attached along the height of beams to measure the concrete strains; these values can be used to find out the strain distribution and the moving neutral axis depth of the beams tested. All beams were loaded in four-point bending to failure with a clear span of 2.7 m, and loading points were located at 450 mm on either side of the mid-span

location. For all beams, the shear-span-to-depth ratios are 4.18 and the length of the bonded plate is 2600 mm, which covers almost the full-span length between the supports of the beams.

The reason for the full-span-length strengthening with FRP plates is to maximize the strengthening effects by delaying the FRP separation. The load was applied step-by-step up to failure in a load control manner of test beams. During the test, the strains on steel and concrete, and vertical deflections were measured using LVDTs. The strain gauges, LVDTs, and the load cell were connected through a data acquisition system to a computer and the data was recorded and stored in the computer. The details of the test specimens and test setup are shown in Figs. 1 and 2.

2.1 Major test variables

The main test variables considered in the present study include the CFRP sheet layers and tensile bars. The CFRP sheet layers varies from 0 to 4 and the bar reinforcement ratio varies from $0.2\rho_b$ to $0.4\rho_b$. Those test variables are summarized in Table 1. Of the six beams tested, two were set aside as control beams and were not strengthened. The remaining four beams were tested in pairs with

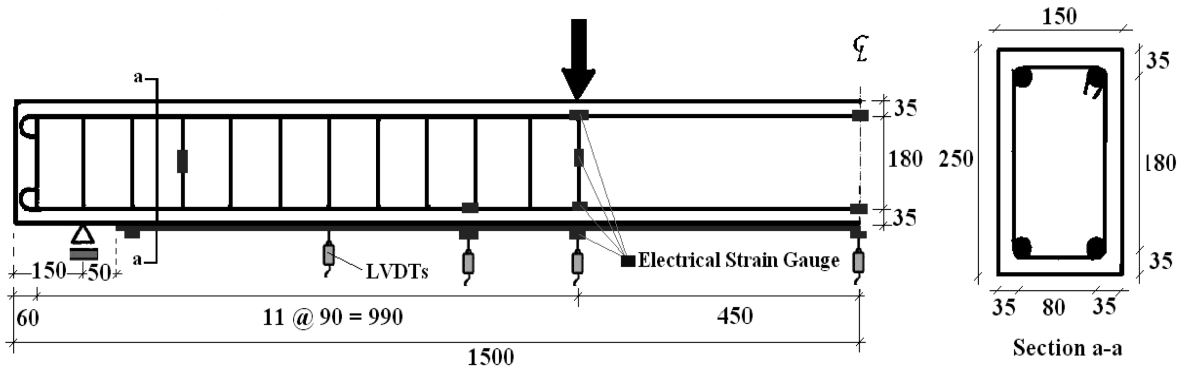


Fig. 1 Beam details and measurement schemes for half of the test specimen (unit: millimeter)

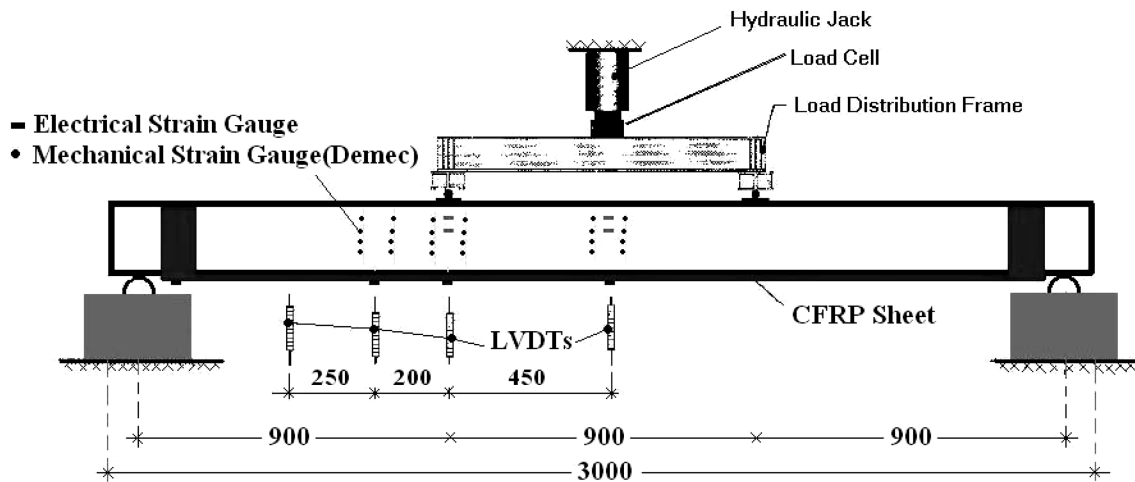


Fig. 2 Details of test setup and measurement schemes (unit: millimeter)

Table 1 Test Parameters and Specimen Identifications

| Series | Test beam | A_S | A'_S | A_{SV} | CFRP layers |
|--------|-----------|-------------|-------------|-----------------|------------------|
| A | AH0 | 2 Φ 16 | 2 Φ 10 | Φ 10 @ 9cm | 0 (control beam) |
| | AH1 | 2 Φ 16 | 2 Φ 10 | Φ 10 @ 9cm | 1 |
| | AH4 | 2 Φ 16 | 2 Φ 10 | Φ 10 @ 9cm | 4 |
| B | BH0 | 2 Φ 22 | 2 Φ 10 | Φ 10 @ 9cm | 0 (control beam) |
| | BH1 | 2 Φ 22 | 2 Φ 10 | Φ 10 @ 9cm | 1 |
| | BH4 | 2 Φ 22 | 2 Φ 10 | Φ 10 @ 9cm | 4 |

Table 2 Mixture proportion of concrete

| Cement (kg/m ³) | Silica fume (kg/m ³) | Coarse agg. (kg/m ³) | Fine agg. (kg/m ³) | Super plasticizer (kg/m ³) | w/c ratio |
|--------------------------------|-------------------------------------|-------------------------------------|-----------------------------------|---|-----------|
| 650 | 55 | 723 | 645 | 11.7 | 0.32 |

different layer of CFRP plate and tensile bar reinforcement ratio. For all beams, the shear-span-to-depth ratios are 4 and the length of the bonded plate is 2,600 mm, which covers almost the full-span length between the supports of the beams (see Fig. 2), and the CFRP plate width is 150 mm which is the same as the beam width.

2.2 Material properties

Mix proportioning of HSC with the maximum size of coarse aggregate, 10 mm is given in Table 2. For each beam three 100 mm×100 mm×100 mm concrete cube specimens were made at the time of casting and were kept with the beams during curing. The average 28-day concrete cube strength (f_{cu}) was 96.2 MPa. The relationship of cylinder strength (f'_c) and cube strength is ($f'_c = 0.8 f_{cu}$) thus the average compressive strength (f'_c) was 77 MPa. Uniaxial compressive tests on produced concrete were performed invariable loading rate of 0.15MPa/s. In these tests, electrical strain-gauge (TML Type) were located on the face of cube specimen in order to measure vertical strain under compression. Strains under compression for each 0.566 MPa stress were recorded and were used to draw stress-strain curves (Fig. 3). Two bars of diameter 16 mm (Φ 16) were tested in tensile and the measured yield strength was 412.5 MPa, and maximum tensile strength was 626.4 MPa. The modulus of elasticity of steel bars was 2×10^5 MPa. The Young's modulus (E_{fu}) and ultimate tensile stress (f_{fu}) of the CFRP sheet materials and the properties of epoxies used for bonding the CFRP sheets were obtained from the supplier and shown in Tables 3, 4.

2.3 CFRP bonding procedure

The concrete surface treatment prior to strengthening was very important to guarantee the perfect bonding between two materials. Prior to bonding of the CFRP sheets, the beams were ground using a mechanical grinder to obtain a clean sound surface, free of all contaminants and then clean with an acetone solution. A two-component structural epoxy was mixed thoroughly in the ratio 1:1 and applied over the concrete surface. The CFRP sheet was installed over the concrete surface by starting at one end and moving along the length of the CFRP sheet until completed. Enough pressure was applied to CFRP sheet. Concrete beams strengthened with CFRP sheets and carbon fiber fabrics were

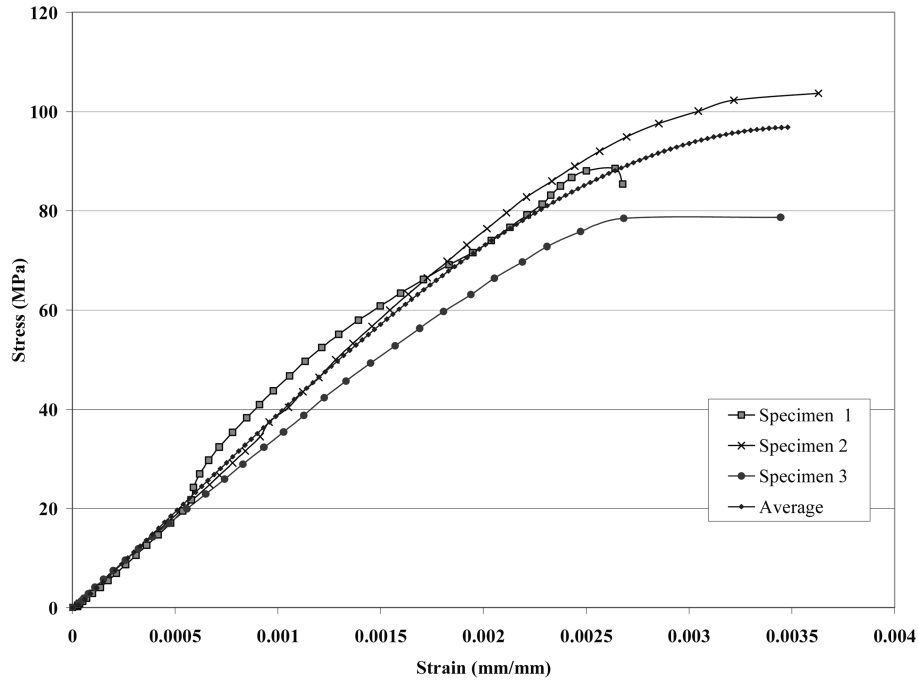


Fig. 3 Stress-strain diagram for high strength concrete

Table 3 Strengthening material properties

| Material | Density (gr/cm ³) | Thickness (mm) | Ultimate tensile stress f_{fu} (MPa) | Young's modulus E_{fu} (GPa) | Ultimate strain ε_{fu} (%) |
|------------|-------------------------------|----------------|--|--------------------------------|--|
| CFRP sheet | 1.78 ± 0.1 | 0.045 | 3850 | 230 | 1.7 ± 0.1 |

Table 4 Epoxy bonding material properties

| Bonding material | Compression strength at 7 day (MPa) | Bending strength at 7 day (MPa) | Bond resistance (MPa) |
|--------------------------|-------------------------------------|---------------------------------|-----------------------|
| Structural epoxy (EP-TX) | >56 | >18 | 2.07 |
| Structural epoxy (EP-IN) | >65 | >45 | 2.07 |

cured for at least seven days at room temperature before testing.

3. Test results and discussions

3.1 Failure modes

The cracking patterns and failure for various test beams are shown in Fig. 4. The control beam without strengthening plates shows the traditional flexural failure because it was designed to fail in flexure. For the control beams (AH0, BH0), failure was by crushing of the concrete in the compression zone after tension steel yield. For the strengthened beams, failure occurred by the rupture

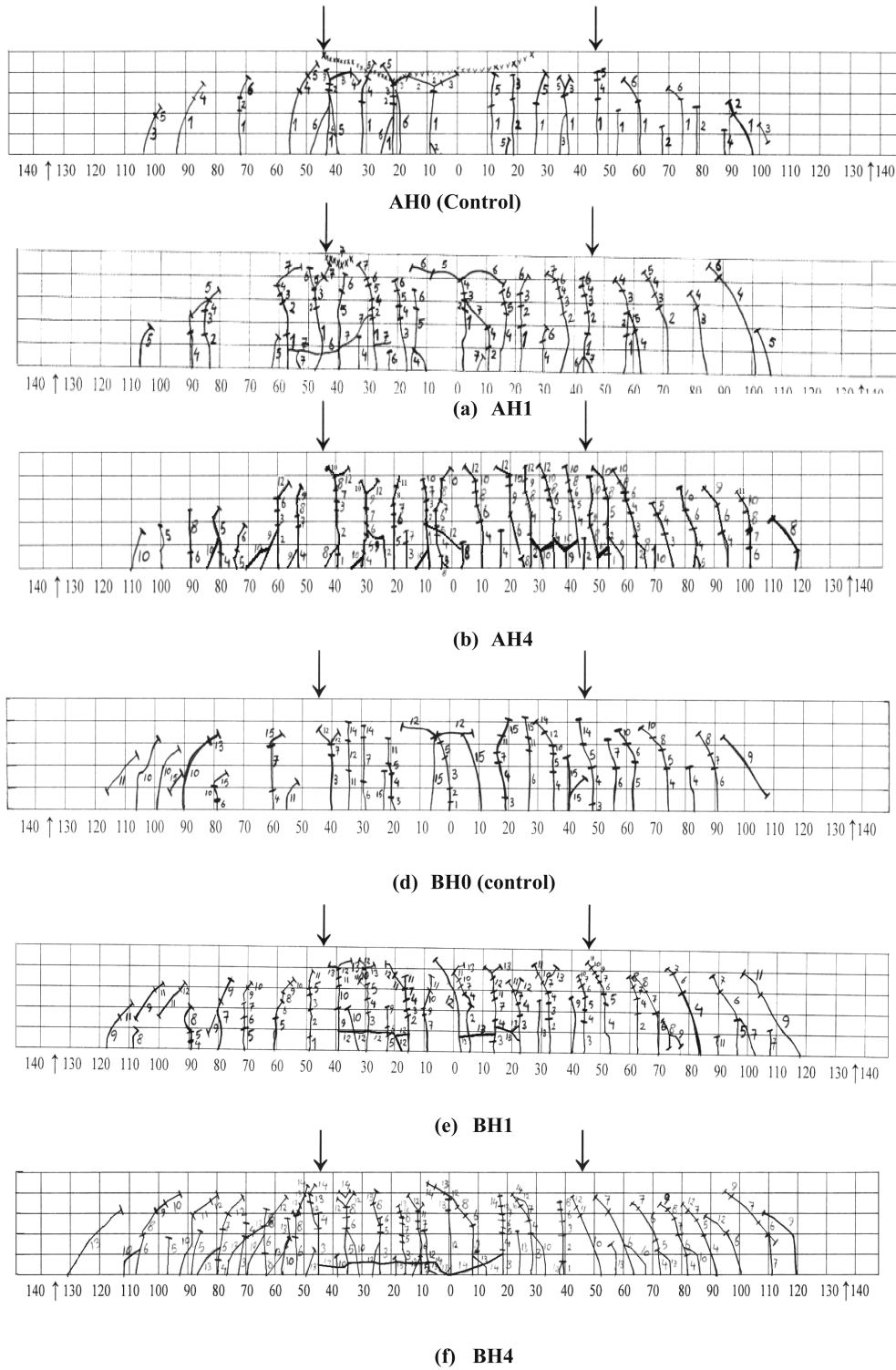


Fig. 4 Failure configuration of control and CFRP beams at ultimate state

of CFRP sheets accompanied by horizontal cracking in the tension zone in the vicinity of the tension steel, as illustrated in Fig. 4. Most of the test beams exhibited the rupture of CFRP sheets and failed in the same manner. We attended to the failure of a concrete cover along the tensile reinforcement. The concrete was not initially precracked and the development of the cracks during the reinforcement test is highly influenced by the number of CFRP layer. The occurrence of first crack was delayed and more diffuse. Shear cracks occurred in the shear span length of the beams for an applied load between 70% to 80% of the ultimate load. Finally the sudden propagation of horizontal cracks in the concrete-steel bond region occurs. This type of cracks runs along the weakest surface, which is the concrete-steel interface. It leads to the failure of the beam as soon as the cracks opened and separates the concrete cover from the rest of the beam.

It is interesting to note that the weakest point of the assemblage concrete-bond-composite material is not the concrete-composite interface but the concrete-internal steel interface. Fig. 4 also indicates that the strengthened beams show many diagonal cracks, which was caused by the increase of flexural capacities due to CFRP sheets. Table 5 summarizes the test results for the peak loads, displacements and strains at the peak loads for the tested beams. Table 5 also shows the increase of peak load according to the various strengthening layers of CFRP. The rates of increase of peak loads varied from 1 to 44% depending upon the strengthening method. The load deflection response for each of the test beams is plotted in Fig. 5. In general, the strengthened beams were stiffer and less ductile than the control specimens with a higher ultimate loads. The tension steel in control beams AH0 and BH0 reached its yield strength before the compressive strain in concrete reached 0.003 and the beams failed by crushing of concrete. Even though the control beams failed by crushing of concrete, since the failure was initiated by yielding of tension steel, the mode of failure was mentioned to be under reinforced tension failure thus the behavior of the two control beams, AH0 and BH0, was a ductile flexural response. For control beams after the first visible cracks observed, the cracking became extensive and crack widths increased steadily. The shape of the load deflection curves indicates a loss of stiffness at a load of approximately 64 kN for AH0 and 122 kN for BH0. This was due to yielding of the tensile reinforcement and occurred at a midspan deflection of 21 mm for AH0 and 13.3 mm for BH0. After this point, large flexural cracks opened during the test and eventual ultimate collapse was by concrete crushing within the compression zone, a photograph of which is presented in Fig. 6. The ultimate loads recorded were 81.25 and 149.5 kN for AH0 and BH0, respectively. In this study, the bond problem is not the controlling factor for failure, thus the force in CFRP will reach its ultimate tensile capacity when the beam fails and the failure mode of the

Table 5 Test Results of the Control and CFRP Strengthened Beams

| Series | Test beam | Failure mode | Peak load P_{ult} (kN) | Ratio to unstrengthened beam | P_{ult} | | | | |
|--------|-----------|-------------------|--------------------------|------------------------------|-------------------|-----------------|---------|----------|------|
| | | | | | Displacement (mm) | Strain (micron) | | | |
| | | | | | CFRP | Tensile rebar | Stirrup | Concrete | |
| A | AH0 | Concrete Crushing | 81.25 | 1 | 102 | - | 2316 | 48 | 3600 |
| | AH1 | CFRP Rupture | 89.96 | 1.11 | 50.42 | 844 | 3341 | 441 | 2500 |
| | AH4 | CFRP Rupture | 117.33 | 1.44 | 32.85 | 2581 | 9557 | 954 | 2100 |
| B | BH0 | Concrete Crushing | 149.52 | 1 | 95.7 | - | 17843 | 644 | 4200 |
| | BH1 | CFRP Rupture | 150 | 1.01 | 63.24 | 1066 | 17330 | 790 | 2600 |
| | BH4 | CFRP Rupture | 167 | 1.12 | 30.92 | 3367 | 4512 | - | 2700 |

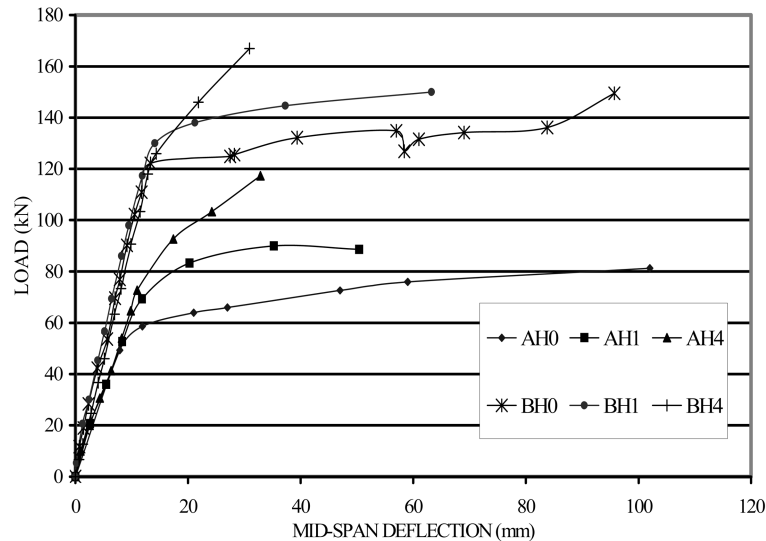


Fig. 5 Load deflection responses of test beams

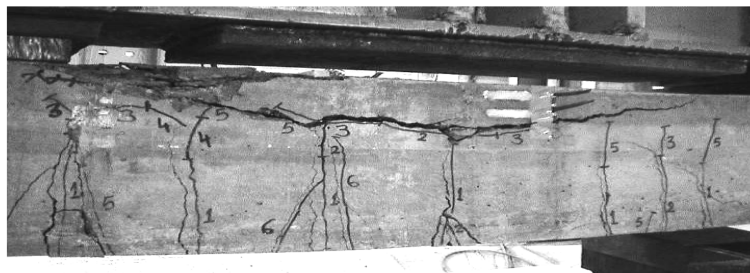


Fig. 6 Flexural failure of control beam AH0

strengthened beams are CFRP rupture in the constant moment region. Figs. 7 and 8 show such a typical failure mode.

Table 6 shows a summary of the flexural behavior of all test beams in terms of flexural loading capacity and deflection. The results are clearly demonstrated the accepted beneficial effects of CFRP layers with regard to stiffening and strengthening of the beams. The strain response of FRPs is different from that of conventional steel, which yields after elastically deforming to relatively small values of strain (0.2% for Grade 60 [410 MPa] and 0.14% for Grade 40 [280 MPa]); FRP materials exhibit elastic deformation to relatively large strain values before rupture. As a result, when FRPs are used for flexural strengthening of concrete beams reinforced with conventional steel, the steel reinforcement may yield before the FRP contributes any additional capacity to the beam. Therefore, it can be difficult to obtain a significant increase in yield load or stiffness for a beam. When an increase in beam yield load or stiffness is required, larger cross sections of FRPs must be used (before the steel yields), which generally increases the cost of strengthening.

Although using some special, low-strain fibers, such as ultra-high-modulus carbon fibers, may appear to be a solution; they can result in brittle failures due to fiber failure. Taking advantage of the high strength of FRPs during flexural strengthening of RC beams is limited by the bond capacity

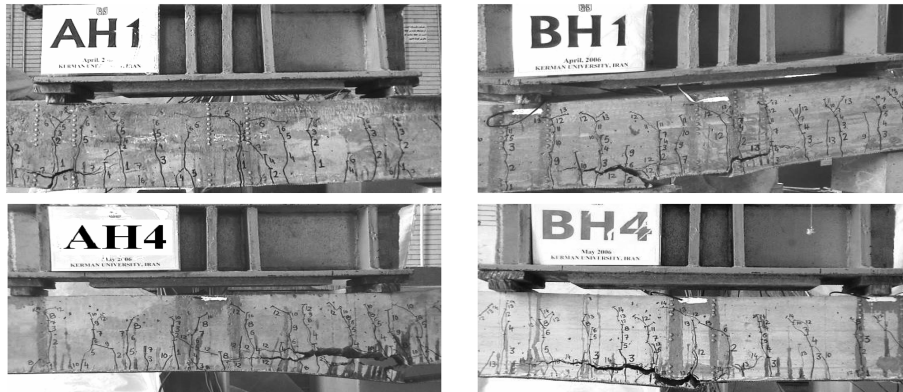


Fig. 7 Rupture of FRP in beams AH1, AH4, BH1 and BH4

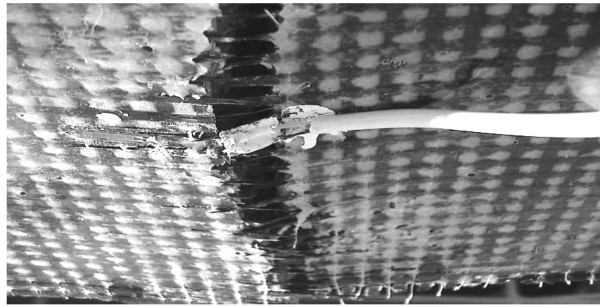


Fig. 8 Closed view of CFRP rupture (bottom of AH1 beam)

Table 6 Test Results for Control and CFRP Strengthened Beams

| Series | Test beam | Yield stage | | | | Ultimate stage | | | |
|--------|-----------|-----------------|---------------------------|-----------------|---------------------------|-----------------|---------------------------|-----------------|---------------------------|
| | | Load P_y (kN) | Increase over control (%) | δ_y (mm) | Decrease over control (%) | Load P_u (kN) | Increase over control (%) | δ_u (mm) | Decrease over control (%) |
| A | AH0 | 63.93 | --- | 21 | --- | 81.25 | --- | 102 | --- |
| | AH1 | 69.5 | 8.7 | 13 | 38 | 89.9 | 11 | 50.42 | 30 |
| | AH4 | 64.7 | 1.2 | 9.83 | 46.8 | 117.3 | 44.4 | 32.85 | 54.5 |
| B | BH0 | 122.2 | --- | 13.325 | --- | 149.52 | --- | 95.7 | --- |
| | BH1 | 130 | 6.4 | 14.11 | -5.9 | 150 | 0.5 | 63.24 | 33.9 |
| | BH4 | 118 | -3.4 | 12.86 | 3.6 | 167 | 11.7 | 30.92 | 67.7 |

between them and the concrete surface. In many cases, debonding occurs (Fanning *et al.* 2001, Malek *et al.* 1998) at stress levels that are a small fraction of the FRPs' strength. As the amount of steel reinforcement increases, the additional strength provided by the carbon FRP external reinforcement decreases. The same amount of CFRP reinforcement more than 44% the flexural strength of a lightly reinforced beam (20% of balanced ratio), but only increased by 11.7% the strength of a moderately reinforced beam (40% of balanced ratio).

3.2 Ductility

Ductility is an important factor for any structural element or structure especially in the seismic regions. A ductile material is one that can undergo large strains while resisting loads. When applied to RC members, the term ductility implies the ability to sustain significant inelastic deformation prior to collapse (Naaman *et al.* 1995). Since CFRP repair is a fairly new innovation and also the HSC behavior is like a brittle material, therefore, understanding the effect of such materials on the ductility of a RC beam is critical. Ductility has generally been measured by a ratio called a ductility index or factor (μ). The ductility index is usually expressed as a ratio of rotation (θ), curvature (ϕ), or deflection (displacement) (δ) at failure to the corresponding property at yielding of steel (Maghsoudi 1996). In the case of beams strengthened with FRP laminates, there is usually no clear yield point. However, it was shown that deflection and energy based on tension steel yielding can be used as a criterion of ductility to evaluate comparative structural performance of FRP bonded RC beams (Mukhopadhyaya *et al.* 1998).

The ductility index in this study is obtained based on deflection (μ_δ) and curvature (μ_ϕ) computation, and is defined as the mid-span deflection or curvature, at peak load, divided by the mid-span deflection or curvature at the point where the steel starts yielding.

Table 6 shows the test results of the beams for yield and ultimate stage and Table 7 shows the experimental deflection and curvature ductility ratio and percent decrease of ductility with respect to the control beam for each of the specimens. For HSC members, displacement ductility, μ_δ , in the range of 3 to 5 is considered imperative for adequate ductility, especially in the areas of seismic design and the redistribution of moments (Maghsoudi *et al.* 2006). Therefore, assuming that a μ_δ value of 3 represents an acceptable lower bound to ensuring the ductile behavior of HSC flexural members, it appears that, for the BH4 beam would not meet that requirement.

3.3 Moment -strain behavior

The relationship between concrete strains (measured on the compression face at mid-span) and applied moments for both A and B series are plotted in Fig. 9. There is a similar increase in strain for all the beams at low moments. However, cracking of the concrete in the tension zone results in larger increments of strain in the control specimens (i.e., for control beam AH0, the extreme layer of concrete compressive strain at failure, $\varepsilon_{\text{cuf}} = 0.0036$). For these beams, concrete strain varies almost linearly with moment, after initial cracking, until yielding of the tension steel. Following

Table 7 Experimental Ductility Ratio of the Test Beams

| Series | Test beam | Deflection ductility ratio | Decrease over control beam (%) | Curvature ductility ratio |
|--------|-----------|---|--------------------------------|---|
| | | $\left(\mu_\delta = \frac{\delta_u}{\delta_y}\right)$ | | $\left(\mu_\phi = \frac{\phi_u}{\phi_y}\right)$ |
| A | AH0 | 4.86 | --- | 6.37 |
| | AH1 | 3.87 | 20.4 | --- |
| | AH4 | 3.34 | 31.3 | 3.91 |
| B | BH0 | 7.19 | --- | 6.2 |
| | BH1 | 4.48 | 37.7 | --- |
| | BH4 | 2.4 | 66.6 | 2.37 |

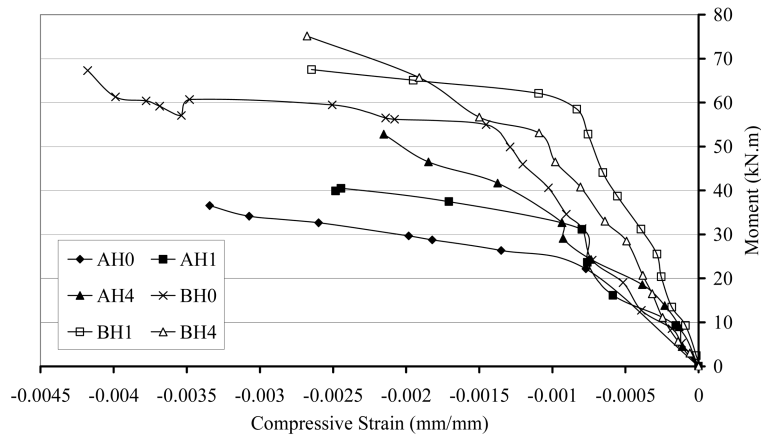


Fig. 9 Moment vs. concrete strain at mid-span of test beams

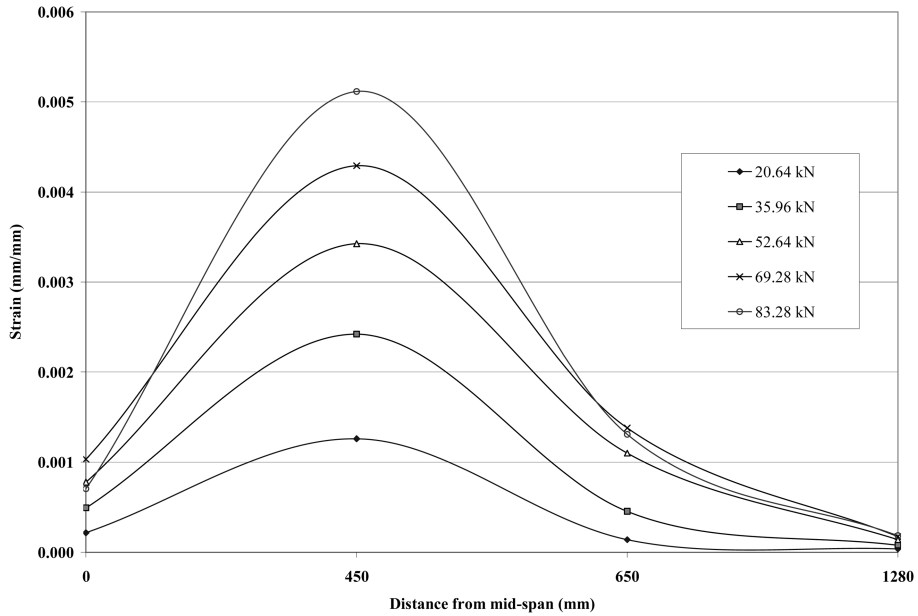
yield, steel strain increases rapidly with each increment of moment, and finally the concrete crushes as the beam collapses (see Table 5).

On the other hand, the extreme compressive strain of concrete fiber in the strengthened beams with the increased number of layers of the carbon fiber sheet, remains more or less linear up to failure of the beam and is not significantly affected by concrete cracking or yielding of the tension steel. These results demonstrate that the effect of the strengthening plate is to reduce strain in the compression fibers of the concrete. The presence of the plate draws the neutral axis lower in the section and, hence, places a greater volume of concrete in compression, resulting in lower strain (see Table 5) and enabling a more efficient use of the existing material. Thus, externally bonded CFRP plates may also be beneficially used to

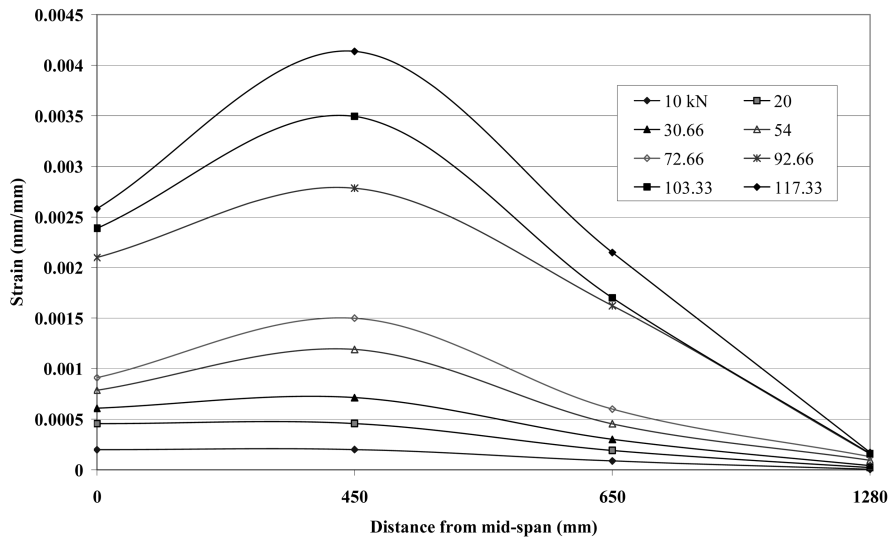
reduce concrete compressive stresses, in addition to acting as additional tensile reinforcement. The variations in longitudinal strain in the CFRP sheet from the mid-span of the beam to the end of the sheet, as a function of the changes in externally applied load are plotted in Fig. 10. Generally the strain in the constant bending moment region was sensibly uniform for a given load, although the strains under the load points, due to the localized loading points, were slightly higher than those recorded at the mid-span. Within the shear span, the strain drops almost linearly from a maximum under the load point to a zero at the end of the sheet. This pattern of strain distribution in the bonded plate was typical of each of the test beams. Similar results are reported by Fanning P. J. *et al.* (2001).

Fig. 11 showed the load vs. strain curves at mid-span of CFRP, tensile steel and extreme top fiber of concrete in beams AH4 and BH4. A positive strain value represents the tension strain in CFRP, tensile steel and a negative strain value indicates the compressive strain in concrete. It can be seen that each curve consists of almost three straight lines with different slopes. The first turning point, A, indicates the cracking of concrete in tension zone. The second turning point, B, refers to the yielding tension steel. The yielding and maximum load (ultimate load) can be found for each beam from its load – strain curve. For beams AH4 and BH4, the tensile steel and CFRP strains are essentially the same at loads below cracking of the concrete.

After cracking, the strains in steel exceeded those of the CFRP laminate. As the load approached the yielding load for the strengthened beam, the strains in steel increased more rapidly than those in the CFRP. This is because the CFRP had begun to debond from the concrete surface nearby cracks.



(a)



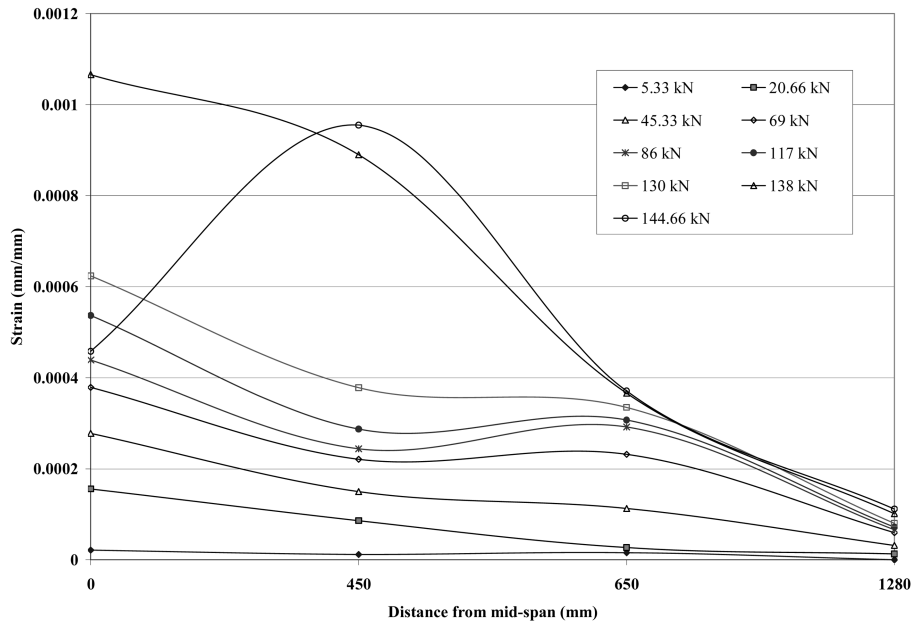
(b)

Fig. 10 CFRP strain distribution for beam

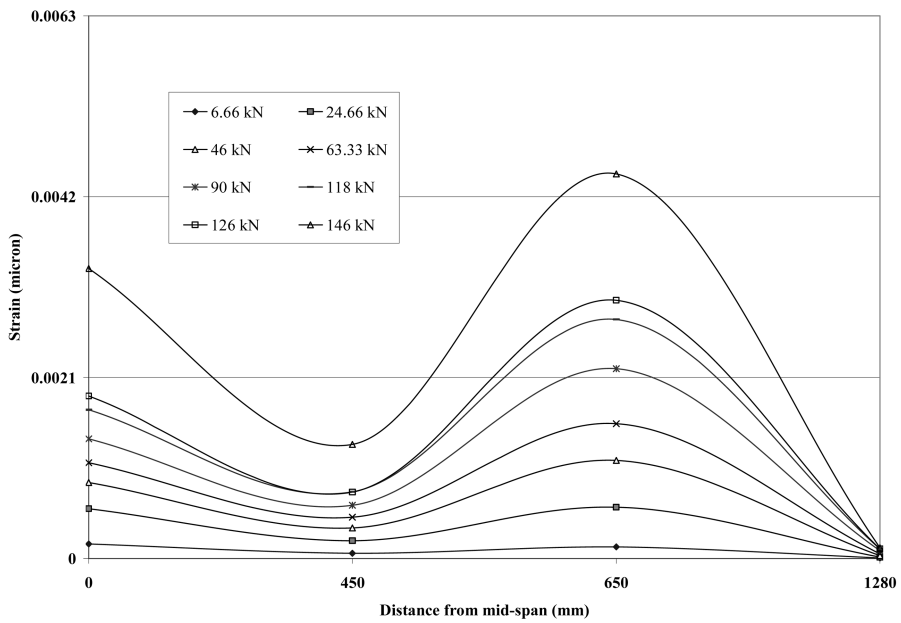
It was noted that the tensile steels strains were always higher than the CFRP strains.

3.4 Analytical study

An analytical procedure, based on compatibility of deformations and equilibrium of forces, is used to predict the flexural behavior of concrete beams strengthened with FRP composites. The following



(c)



(d)

Fig. 10 Continued

assumptions are made in the formulations: (1) strain distribution along the depth of the beam section is linear; (2) shear deformation is small; (3) perfect bond exists between concrete surface and FRP sheets/fabric; (4) contribution of concrete in tension is ignored and (5) failure of the beam

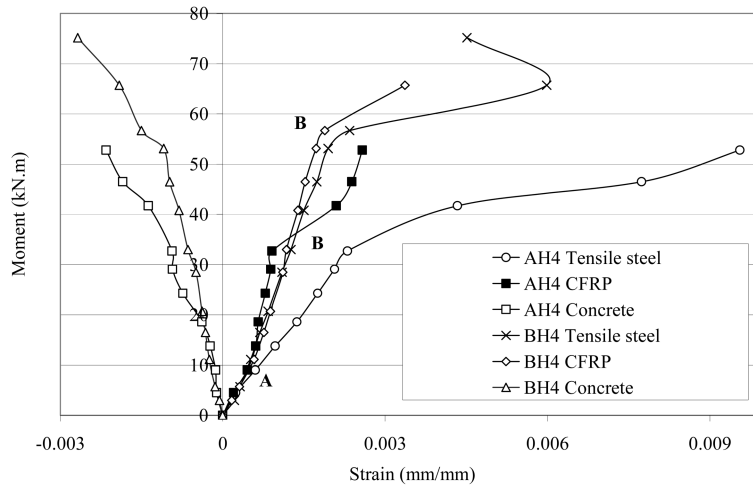


Fig. 11 Moment-strain curves of CFRP, tensile steel and extreme top concrete fiber for beams AH4 and BH4

occurs when either the compressive strain in the concrete reaches 0.003 or the tensile strain in the FRP composites reaches its ultimate strain. This model ignores the failure of beams due to debonding of CFRP sheets/carbon fiber fabric. In this study, the reinforcing steel is assumed to be elastic-plastic, and a linear stress and strain relationship is considered for FRP sheets/fabric.

3.5 Theoretical stress and strain calculation

For test beams, the strain and stress in the FRP plate, steel rebar, and concrete at mid-span section, are calculated using an incremental deformation technique described in the following.

Fig. 12 shows the strain, stress and the force diagram for a typical rectangular beam with a composite plate bonded to the tension face. The strain in the extreme compressive fiber of concrete at mid-span (ϵ_{cf}), is increased until failure is reached. It is assumed that, failure is reached when either the concrete strain reaches 0.003 or the composite plate reaches its ultimate strain. Next,

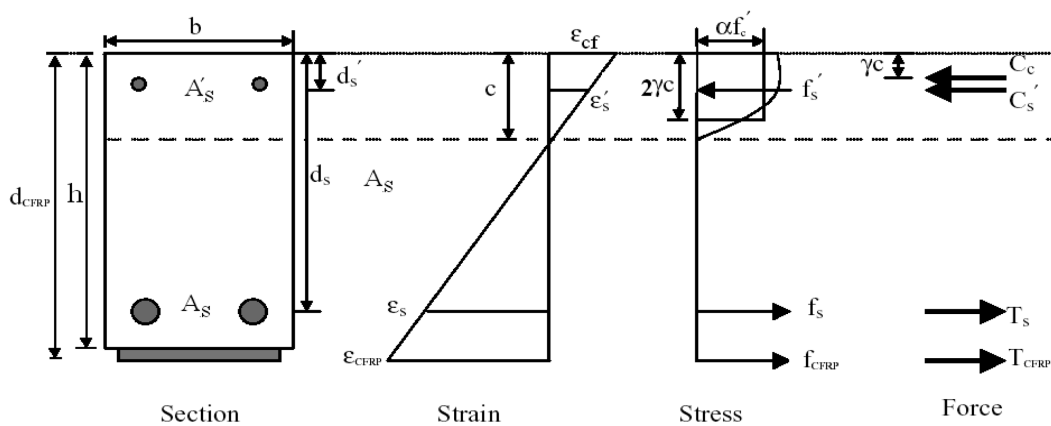


Fig. 12 Strain, stress, and force diagrams across depth of rectangular section

strains in the tensile steel and composite plate are calculated in terms of ε_{cf} from the following equations

$$\varepsilon'_s = \frac{c - d'_s}{c} \times \varepsilon_{cf} \quad (1)$$

$$\varepsilon_s = \frac{d_s - c}{c} \times \varepsilon_{cf} \quad (2)$$

$$\varepsilon_{FRP} = \frac{d_{FRP} - c}{c} \times \varepsilon_{cf} \quad (3)$$

The following are equations for the stresses of the CFRP and reinforcing steel, and are obtained from their stress-strain behavior

$$\text{if } 0 \leq \varepsilon'_s < \varepsilon_y \rightarrow f'_s = E_s \times \varepsilon'_s \quad \text{otherwise} \quad f'_s = f_y \quad (4)$$

$$\text{if } 0 \leq \varepsilon_s < \varepsilon_y \rightarrow f_s = E_s \times \varepsilon_s \quad \text{otherwise} \quad f_s = f_y \quad (5)$$

$$f_{FRP} = E_{FRP} \times \varepsilon_{FRP} \quad (6)$$

Each of the corresponding internal forces can be determined by multiplying the stress by their cross-sectional areas. Hence, the forces are as follows

$$C'_s = f'_s \times A'_s \quad (7)$$

$$T_s = f_s \times A_s \quad (8)$$

$$T_{frp} = f_{frp} \times A_{frp} \quad (9)$$

For any given concrete strain in the extreme compression fiber ε_{cf} , the concrete compression force C_c is expressed in terms of a parameter α , defined as follows (Park and Paulay 1975)

$$C_c = \alpha \times f'_c \times b \times c \quad (10)$$

3.6 Determination of stress block parameters

The distribution of concrete stresses in the compression zone is found from the stress-strain curve of concrete. Stress-strain model produced by Hognestad is one of the most commonly used for ordinary concrete that the initial part of the concrete compression stress-strain relationship is represented by a second order parabolic expression up to the maximum concrete stress and the falling branch is linear. Fig. 13 shows the concrete stress-strain curve when f'_c = concrete compressive strength; σ_c = stress in concrete; ε_c = extreme layer of concrete compressive strain. In this study, some regulations were made on the Hognestad's model for high performance concrete using stress-strain relation obtained from experimental data. In these regulations, the area of stress-strain curve, total compressive force and application point of the total compressive force are the same as the curves obtained by experimental studies.

The stress-strain curve for ordinary concrete has been defined by Hognestad is given below

$$\sigma_c = f'_c \left[\frac{2\varepsilon_c}{\varepsilon_{co}} - \left(\frac{\varepsilon_c}{\varepsilon_{co}} \right)^2 \right] \quad (11)$$

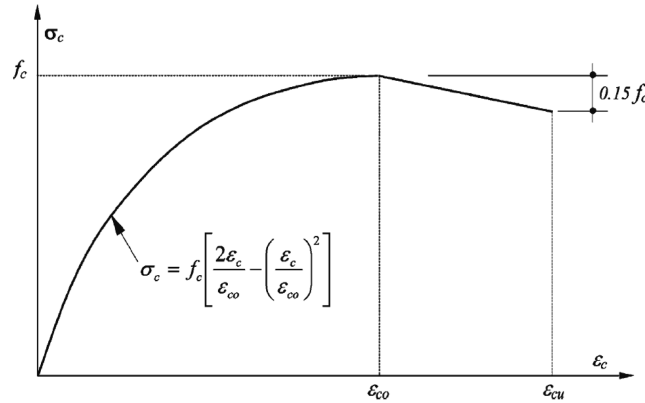


Fig. 13 Stress-strain curve for ordinary concrete in uniaxial compression proposed by Hognestad *et al.* (1995)

High performance concrete specimens are fractured suddenly and brittle when they reach ultimate stress under uniaxial compression. Thus, to define the falling branch of stress-strain curve is very difficult. In the regulations on the Hognestad Model, it is assumed that ultimate strain equals strain in the maximum stress ($\varepsilon_{co} = \varepsilon_{cu}$) in this study. Thus, the equations given below are valid while $\varepsilon_c \leq \varepsilon_{cu}$.

If $k\left(\frac{\varepsilon_c}{\varepsilon_{cu}}\right)$ is written instead of $\frac{2\varepsilon_c}{\varepsilon_{co}}$ and $(k-1)\left(\frac{\varepsilon_c}{\varepsilon_{cu}}\right)^2$ is written instead of $\left(\frac{\varepsilon_c}{\varepsilon_{co}}\right)^2$ in Eq. (11), the modified Eq. (12) is obtained for high performance concrete as

$$\sigma_c = f_c \left(k \frac{\varepsilon_c}{\varepsilon_{cu}} - (k-1) \left(\frac{\varepsilon_c}{\varepsilon_{cu}} \right)^2 \right) \quad (12)$$

Stress-strain curve of high performance concrete are more linear than ordinary concrete's. So, Eq. (13) is used to get more linear curve for high performance concrete (Oztekkin *et al.* 2003).

$$k = 2 - [(f_c - 40)/70] \quad 60 \text{ MPa} \leq f_c \leq 94 \text{ MPa} \quad (13)$$

ε_{cu} , proposed by Oztekkin *et al.* (2003) as follow

$$\varepsilon_{cu} = [2.2 + 0.015(f_c - 40)] \times 10^{-3} \quad 60 \text{ MPa} \leq f_c \leq 94 \text{ MPa} \quad (14)$$

In this study according to experimental result (Fig. 3), the value of ε_{cu} is assumed to be equal to 0.003 (i.e., similar to suggested value by ACI 05).

Hognestad's, Oztekkin *et al.* (2003) modified, proposed model and experimental stress-strain curves are shown in Fig. 14. It is known that real stress distribution in compressive area at a cross section is the same as the stress-strain curve in uniaxial compression. But stress-strain curve is affected by a lot of variables. Therefore, it is not easy to suggest a certain stress-strain curve for concrete. Perhaps the area of stress-distribution and its centre of gravity are more important than the geometry of the stress distribution for equilibrium equation in RC design. So, rectangular stress block, which is suggested by ACI-318 (1989), is preferred for ease of calculation of area, centre of gravity and others. The design method given for ordinary concrete by ACI-318 (1989) can be valid for high strength concrete but rectangular stress block parameters should be obtained for high strength

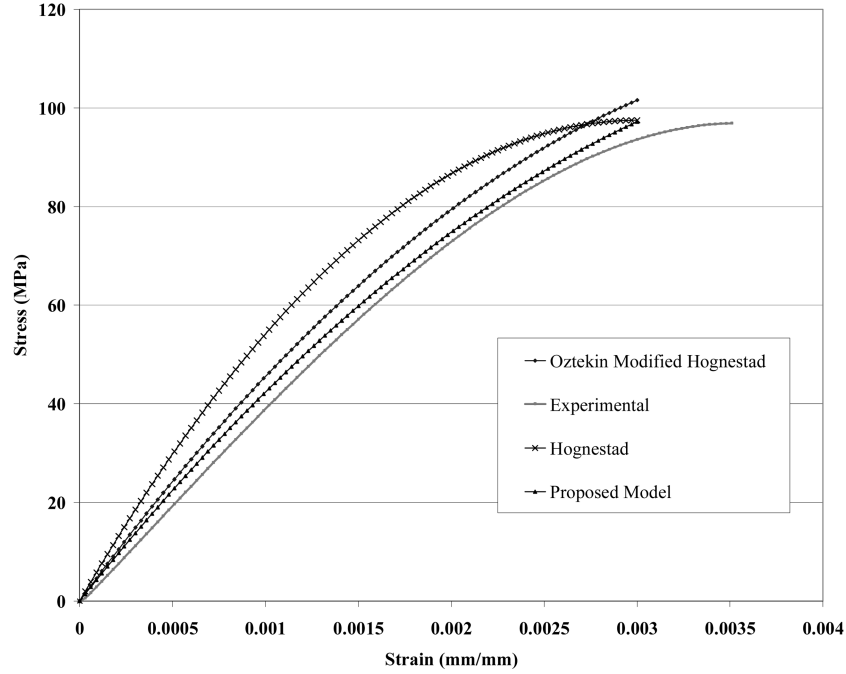


Fig. 14 Hognestad's oztekin, proposed model and experimental stress-strain curves for compressive concrete

concrete again. So stress block parameters used in calculations have been developed using a modified Hognestad model for high performance concrete in this study.

In this study, a new stress block model is constituted to obtain stress-strain parameters for calculation for high performance concrete. The parameter α (stress factor) is used to convert the actual concrete stress into an equivalent rectangular stress block. This is usually calculated by equating the area of under stress-strain curve to an equivalent rectangular area

$$A = \int_0^{\varepsilon_{cf}} \sigma_c d\varepsilon_c = \alpha f_c \varepsilon_{cf} \quad (15)$$

where A = area under stress-strain curve of concrete.

then, α is obtained by

$$\alpha = \frac{\int_0^{\varepsilon_{cf}} \sigma_c d\varepsilon_c}{f_c \varepsilon_{cf}} \quad (16)$$

Evaluating the right side of Eq. (15), results in the following values for α

$$\alpha = \frac{\varepsilon_{cf}(-2k\varepsilon_{cf} + 2\varepsilon_{cf} + 3k\varepsilon_{cu})}{6\varepsilon_{cu}^2} \quad \text{if } 0 \leq \varepsilon_{cf} < \varepsilon_{cu} \quad (17)$$

The position of concrete compressive force C_c , measured from the top fiber of concrete, is expressed in terms of the parameter γ calculated as follows

$$d_c = \gamma \times c \quad (18)$$

where d_c = distance from top concrete fiber to line of action of concrete compressive force.

The first moment of area under the actual concrete stress-strain diagram is given by

$$Q = \int_0^{\varepsilon_{cf}} \sigma_c \varepsilon_c d\varepsilon_c = \bar{\varepsilon}_c A \quad (19)$$

where $\bar{\varepsilon}_c$ = strain at centroid of area under stress-strain diagram.

The strain $\bar{\varepsilon}_c$ can be defined in terms of ε_{cf} by

$$\bar{\varepsilon}_c = (1 - \gamma) \varepsilon_{cf} \quad (20)$$

and therefore

$$Q = \bar{\varepsilon}_c A = (1 - \gamma) \varepsilon_{cf} \int_0^{\varepsilon_{cf}} \sigma_c d\varepsilon_c \quad (21)$$

The parameter γ (centroid factor) is obtained by equating Eqs. (19) and (21)

$$\gamma = 1 - \frac{\int_0^{\varepsilon_{cf}} \varepsilon_c \sigma_c d\varepsilon_c}{\varepsilon_{cf} \int_0^{\varepsilon_{cf}} \sigma_c d\varepsilon_c} \quad (22)$$

Evaluating Eq. (22), results in the following values for γ

$$\gamma = \frac{-0.5k\varepsilon_{cf} + 0.5\varepsilon_{cf} + k\varepsilon_{cu}}{-2k\varepsilon_{cf} + 2\varepsilon_{cf} + 3k\varepsilon_{cu}} \quad \text{if } 0 \leq \varepsilon_{cf} < \varepsilon_{cu} \quad (23)$$

The location of the neutral axis, c , is obtained from the equilibrium of internal forces as given by Eq. (24). Eq. (24) is solved iteratively until the equilibrium of forces across the depth of the cross section is satisfied

$$\alpha f_c b c + f_s' A_s' = f_s A_s + f_{FRP} A_{FRP} \quad (24)$$

If no FRP is used (control beam), zero is inserted for the area of the FRP (A_{FRP}).

Next, by substituting Eq. (1) through Eq. (6) into Eq. (24), the neutral axis depth can be calculated using the quadratic equation. With this parameter known, the internal resisting moment (M) of the section can be obtained by taking the sum of the moments about the middle height of the section

$$M = \alpha f_c b c \left(\frac{h}{2} - \gamma c \right) + f_s' A_s' \left(\frac{h}{2} - d_s' \right) + f_s A_s \left(d_s - \frac{h}{2} \right) + f_{FRP} A_{FRP} \left(d_{FRP} - \frac{h}{2} \right) \quad (25)$$

3.7 Theoretical curvature calculation

As before, the curvature at mid-span section of the beam can be calculated using an incremental deformation technique. The beam curvature is determined by considering a small element, dx , subjected to pure bending moments, as shown in Fig. 15 (Park and Paulay 1975). The radius of curvature (R), the neutral axis from the extreme compressive fiber, the concrete strain of the extreme compression fiber,

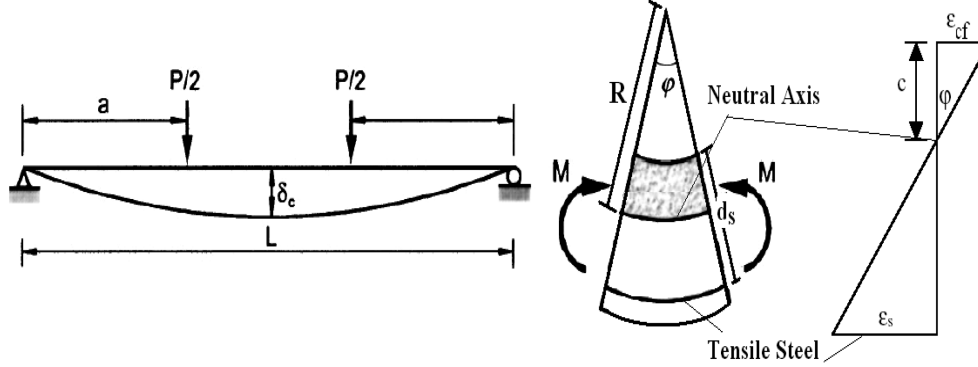


Fig. 15 Central displacement and moment curvature relationship

and the tension steel strain, all change under loading. Assuming plane sections remain plane (linear behavior), the rotation between the ends of the element can be described by the following:

$$\frac{dx}{R} = \frac{\varepsilon_{cf} dx}{c} = \frac{\varepsilon_s dx}{d_s - c} \Rightarrow \frac{1}{R} = \frac{\varepsilon_{cf}}{c} \quad (26)$$

Therefore, the curvature at mid-span is calculated by dividing the concrete strain by ε_{cf} by a distance to the neutral axis depth, c

$$\phi = \frac{\varepsilon_{cf}}{c} \quad (27)$$

The deflections at mid-span of the beams can be calculated by employing the relation between the displacement and the curvature. The mid-span displacement for the two-point loading of Fig. 15 is expressed as

$$\delta_c = \frac{pa}{48EI} (3L^2 - 4a^2) \quad (28)$$

$a = \frac{L}{3}$ in this study, therefore Eq. (28) can be rewritten as

$$\delta_c = \frac{23 \times PL^3}{1296 \times EI} \quad (29)$$

By using the relationship between of curvature and moment, i.e., $\phi = \frac{M}{EI}$, and by employing $M = \frac{PL}{6}$ for the shown load case, the central deflection i.e., Eq. (29), can be rewritten as

$$\delta_c = \frac{23L^2}{216} \frac{M}{EI} = \frac{23L^2}{216} \phi \quad (30)$$

3.8 Application of model

A spreadsheet was created to predict the behavior of the strengthened RC specimens. When a value for the extreme compressive concrete strain fiber is entered, the program will calculate the strain, for the compressive and tensile steel reinforcement, CFRP strain, also the curvature, moment, and deflection. The predicted yielding load, ultimate load, deflection at the points where the steel reinforcement begins to yield and at the maximum capacity are listed in Table 8 for each of the

Table 8 Comparisons between experimental and predicted theoretical values

| Series | Test beam | Yield stage | | | | Ultimate stage | | | |
|--------|-----------|--------------|-----------------|------------|-----------------|----------------|-----------------|------------|-----------------|
| | | Experimental | | Analytical | | Experimental | | Analytical | |
| | | P_y (kN) | δ_y (mm) | P_y (kN) | δ_y (mm) | P_y (kN) | δ_y (mm) | P_u (kN) | δ_u (mm) |
| A | AH0 | 63.93 | 21 | 71.95 | 11.12 | 81.25 | 102 | 78.12 | 109 |
| | AH1 | 69.5 | 13 | 74.03 | 10.85 | 89.9 | 50.42 | 85.95 | 46.7 |
| | AH4 | 64.7 | 9.83 | 79.6 | 10.18 | 117.3 | 32.85 | 111.8 | 42.07 |
| B | BH0 | 122.2 | 13.325 | 131.4 | 11.48 | 149.52 | 95.7 | 138.2 | 76.71 |
| | BH1 | 130 | 14.11 | 133.26 | 11.33 | 150 | 63.24 | 142.73 | 32.3 |
| | BH4 | 118 | 12.86 | 137.64 | 11 | 167 | 30.92 | 179.8 | 50.6 |

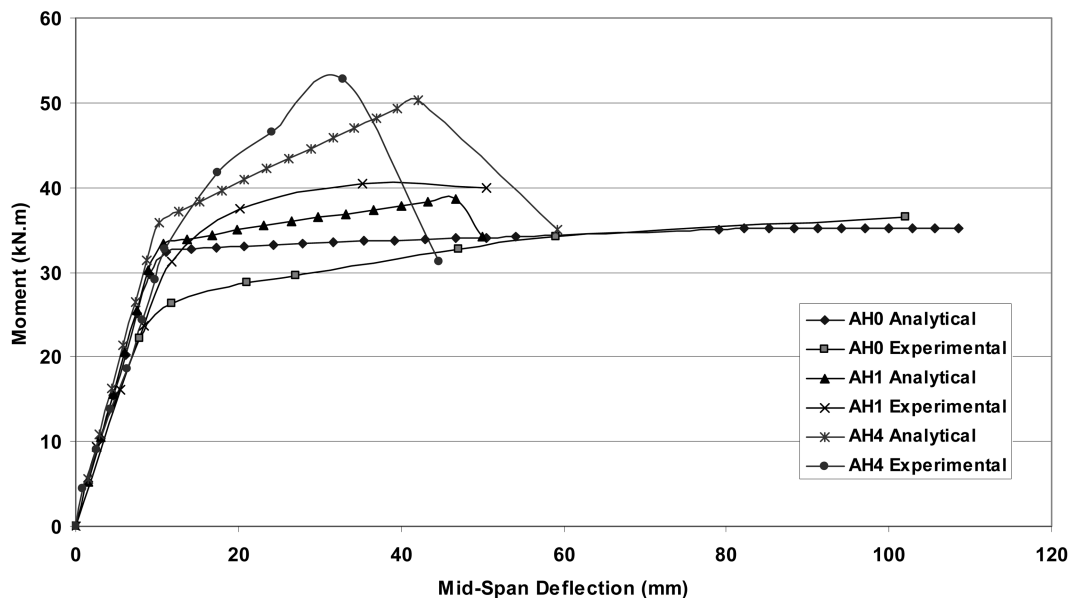


Fig. 16 Comparison between experimental and predicted moment-deflection curves for a series beam

specimens. Plots were generated by increasing the concrete strain in increments of 0.0001 mm/mm until the ultimate strain of either the concrete or CFRP was reached. Fig. 16 show the theoretical moment-deflection curve for the A series of test beams. The figure show very little difference in the behavior of the specimen with CFRP applied until the steel reinforcement begins to yield.

After this point, the moment increases and the deflection decreases proportionally to the number of FRP layers that are applied. Failure of the beams occurs when either the compressive strain in concrete reaches 0.003 or the tensile strain in the CFRP composites reaches its ultimate strain. However this model ignores the failure of beams due to debonding of CFRP sheets. As shown in Fig. 16, the agreement between experimental data and theoretical prediction is close for yielding and ultimate stage thus the proposed model predicts the load and deflection very well. The theoretical model ignores concrete in tension, and consequently is less stiff than the measurements at low values of moment, before concrete cracks in tension. The model also dose not predict debonding failure, and therefore allows the carbon to increase in strain up to 1.5%, close to its rupture strain.

Table 9 Comparisons of experimental and predicted moment and deflection for other studies

| Ref. | Test beam | Yield stage | | | | Ultimate stage | | | |
|-------------------------------------|-----------|-----------------|--------------------|-----------------|--------------------|-----------------|--------------------|-----------------|--------------------|
| | | Experimental | | Prediction | | Experimental | | Prediction | |
| | | M_y (kN.m) | δ_y (mm) | M_y (kN.m) | δ_y (mm) | M_u (kN.m) | δ_u (mm) | M_u (kN.m) | δ_u (mm) |
| Balaguru <i>et al.</i> (1997) | IS1 | 36.7 | 13 | 38.7 | 11.8 | 40.2 | 20.1 | 38.7 | 22.5 |
| | IS2 | 37.8 | 12.9 | 39.1 | 12.1 | 46 | 23.3 | 44.3 | 23.2 |
| | IS3 | 42.3 | 14 | 42.8 | 12.1 | 55 | 24.1 | 53.1 | 24.9 |
| Spadea <i>et al.</i> (1998) | A3-1 | 54.9 | 32 | 56.8 | 30.5 | 67.3 | 61 | 68.8 | 65.9 |
| | A3-2 | 55.1 | 32 | 56.8 | 30.5 | 89 | 135 | 83.6 | 117.9 |
| | A3-3 | 55 | 32 | 56.8 | 30.5 | 88.4 | 115 | 84.7 | 122.4 |
| Toutanji <i>et al.</i> (2006) | CB | 7.5 | 6.5 | 7.7 | 6.4 | 10.4 | 34.3 | 10.8 | 36.2 |
| | 3L-1 | 11.4 | 7.1 | 11.7 | 6.5 | 14.8 | 12.4 | 13.9 | 12.1 |
| | 4L-1 | 13.2 | 7.2 | 13.9 | 6.4 | 15.6 | 12.6 | 15.2 | 12.2 |
| | 4L-2 | 12.2 | 6.8 | 13.9 | 6.4 | 15.4 | 13.5 | 15.2 | 12.2 |
| | 5L-1 | 13.7 | 6.5 | 13.6 | 6.5 | 17.6 | 12.8 | 17 | 12.5 |
| | 5L-2 | 14.3 | 7 | 13.6 | 6.5 | 17.3 | 13.5 | 17 | 12.5 |
| | 6L-1 | 14.4 | 7.1 | 14.1 | 6.3 | 17.8 | 12.1 | 18.6 | 12.8 |
| 6L-2 | 14.9 | 7.3 | 14.1 | 6.3 | 17.6 | 12.1 | 18.6 | 12.8 | |

3.9 Verification of the proposed model using other studies

To testify the proposed model, some previous studies on the flexural behavior of RC beams strengthened by CFRP are selected. Balaguru *et al.* (1997) studied and compared the strengthening effect of inorganic and organic matrix systems. In the research by Balaguru *et al.* (1997), two, three and five layers of carbon fiber were used (IS1, IS2 & IS3) and tested under four-point flexural loading. They reported that beams strengthened with inorganic matrix had higher post-yield stiffness than those with the equivalent organic system, and all failed by fiber rupture.

Spadea *et al.* (1998) tested three beams (A3-1, A3-2 & A3-3) bonded with FRP plate and external anchorage and failure strain in FRP were recorded. In the study by Toutanji *et al.* (2006), three to six layers of carbon fiber were applied to RC beams (3L, 4L, 5L & 6L) with an inorganic matrix. From the test result, it was found that the load carrying capacity of the RC beams increased with the number of layers of the carbon fiber sheet. For three and four layers of FRP reinforcement, beams failed by the rupture of carbon fiber sheet; for five and six layers of FRP reinforcement, beams failed by FRP delamination. Their study show that the ductility of strengthened beams is greatly reduced compared to the control beam. Comparisons have shown that the proposed model agrees very well with the experimental moment and deflection, justifying the use of the proposed model, as can be seen in Table 9.

4. Conclusions

Four-point bending flexural tests were conducted on two concrete control beams and four concrete beams strengthened with externally bonded CFRP sheets. An analytical procedure, based on compatibility of deformations and equilibrium of forces, was presented. The effectiveness of

externally bonded CFRP sheets on the flexural strength of HSC beams was studied. The mid-span deflections at yield load and at failure load, the maximum strain in the CFRP sheets at failure, the variation of stress in the CFRP sheets along the span length at failure load, and the failure load were calculated and compared with experimental results. The failure load of the strengthened beams was also calculated using with the analytical procedure. The results of tests performed in this study indicate that significant increase in the flexural strength can be achieved by bonding CFRP sheets to the tension face of high strength reinforced concrete beams. The gain in the ultimate flexural strength was more significant in beams with lower steel reinforcement ratios.

In addition, strengthening reduced crack width in the beams at all load levels. Strengthening somewhat reduced the ductility of the beams. This reduction in ductility varies with the ductility of the original beam and must be considered in the design especially in the seismic areas. Compared to a beam reinforced heavily with steel only, beams reinforced with both steel and CFRP have adequate deformation capacity, in spite of their brittle mode of failure. As the amount of tensile steel reinforcement increases, the additional strength provided by the carbon FRP external reinforcement decreases. The same amount of CFRP reinforcement more than 44.4% the flexural strength of a lightly reinforced beam (20% of balanced ratio), but only increased by 11.7% the strength of a moderately reinforced beam (40% of balanced ratio). A comparison of the measured results and analytical results based on the equilibrium of forces and compatibility of deformations indicated that the behavior of upgraded beams can be predicted with reasonable accuracy.

References

- ACI Committee 318 (1989), "Building code requirements for reinforced concrete", *American Concrete Institute*, Detroit.
- ACI (1992), "State-of-the-art report on high-strength concrete", ACI 363R, Detroit. An, W., Saadatmanesh, H. and Ehsani, M.R. (1991), "RC beams strengthened with FRP plates II: Analysis and parametric study", *J. Struct. Eng.*, **117**(11), 3434-3455.
- Balaguru, P. and Kurtz, S. (1997), "Use of inorganic polymer-fiber composites for repair and rehabilitation of infrastructures", *Proceeding of the International Conference on Repair and Rehabilitation of Reinforced Concrete Structures*, 155-168.
- Burg, R.G. and Ost, B.W. (1992), "Engineering properties of commercially available high-strength concretes", *PCA Research & Development Bull*, RD104T, Portland Cement Association, Skokie, Ill.
- Buyukozturk, O. and Hearing, B. (1998), "Failure behavior of precracked concrete beams retrofitted with FRP", *J. Compos. Constr.*, **2**(3), 138-144.
- Carrasquillo, R.L., Nilson, A.H. and Slate, F.O. (1981), "Properties of high strength concrete subject to short-term loads", *J. Am. Concr. Inst.*, **78**(3), 171-178.
- Fanning, P.J. and Kelly, O. (2001), "Ultimate response of RC beams strengthened with CFRP plates", *J. Compos. Constr.*, **5**(2), 122-127.
- Fédération Internationale de la Précontrainte/Comité Euro-International du Béton (FIP/CEB), (1990), "High strength concrete: State of the art report", *Bull. d'Information No. 197*, London.
- GangaRao, H.V.S. and Vijay, P.V. (1998), "Bending behavior of concrete beams wrapped with carbon fabric", *J. Struct. Eng.*, **124**(1), 3-10.
- Grace, N.F., Sayed, G.A., Soliman, A.K. and Saleh, K.R. (1999), "Strengthening reinforced concrete beams using fiber reinforced polymer (FRP) laminates", *ACI Struct. J.*, **96**(5), 865-874.
- Hognestad, E., Hanson, N.W. and McHenry, D. (1955), "Concrete stress distribution in ultimate strength design", *ACI J., Proceedings*, **52**(12), 455-479.
- Maghsoudi, A.A. and Akbarzadeh, H. (2006), "Flexural ductility of HSC members", *Struct. Eng. Mech.*, **24**(2),

- 195-213.
- Maghsoudi, A.A. (1996), "Design for ductility of structures", *Shaheed Bahonar University Publications*, Kerman, Iran.
- Malek, A.M., Saadatmanesh, H. and Ehsani, M.R. (1998), "Prediction of failure load of R/C beams strengthened with FRP plate due to stress concentration at the plate end", *ACI Struct. J.*, **95**(2), 142-152.
- Mansur, M.A., Wee, T.H. and Chin, M.S. (1994), "Some engineering properties of locally produced high-strength concrete", *Proc., 19th Conf. on our World in Concrete and Structures*, CI-Premier Pte. Ltd., Singapore, 97-106.
- Mukhopadhyaya, P., Swamy, N. and Lynsdale, C. (1998), "Optimizing structural response of beams strengthened with GFRP plates", *J. Compos. Constr.*, **2**(2), 87-95.
- Naaman, A. and Joeng, S. (1995), "Structural ductility of concrete prestressed beams with FRP tendons", *Proceeding of the Second International RILEM Symposium – Non Metallic (FRP) Reinforcement for Concrete Structures*, Ghent, Belgium, 379-386.
- Oztekin, E., Pul, S. and Husem, M. (2003), "Determination of rectangular stress block parameters for high performance concrete", *J. Eng. Struct.*, **25**, 371-376.
- Park, R. and Paulay, T. (1975), "Reinforced concrete structures", Wiley, New York. Paster, J.A., Nilson, A.H. and Slate, F.O., "Behavior of high-strength concrete beams", Report No. 84-3, *Department of Structural Engineering*, Cornell University, Ithaca, NY, Feb, 1984, 311.
- Rabinovitch, O. and Frostig, Y. (2000), "Closed-form high-order analysis of RC beams strengthened with FRP strips", *J. Compos. Constr.*, **4**(2), 65-74.
- Rahimi, H. and Hutchinson, A. (2001), "Concrete beams strengthened with externally bonded FRP plates", *J. Compos. Constr.*, **5**(1), 44-56.
- Rashid, M.A., Mansur, M.A. and Paramasivam, P. (2002), "Correlations between mechanical properties of high-strength concrete", *J. Mater. Civil Eng.*, **14**(3), 230-238.
- Ross, C.A., Jerome, D.M., Tedesco, J.W. and Hughes, M.L. (1999), "Strengthening of reinforced concrete beams with externally bonded composite laminates", *ACI Struct. J.*, **96**(2), 212-220.
- Saadatmanesh, H. and Ehsani, M.R. (1991), "RC beams strengthened with GFRP plates, I: Experimental study", *J. Struct. Eng.*, **117**(11), 3417-3433.
- Sharif, A., Al-Sulaimani, G.J., Basunbul, I.A., Baluch, M.H. and Ghaleb, B.N. (1994), "Strengthening of initially loaded reinforced concrete beams using FRP plates", *ACI Struct. J.*, **91**(2), 160-168.
- Sonobe, Y. *et al.* (1997), "Design guidelines of FRP reinforced concrete building structures", *J. Compos. Constr.*, **1**(3), 90-115.
- Spadea, G., Bencardino, F. and Swamy, R.N. (1998), "Structural behavior of composite RC beams with externally bonded CFRP", *J. Compos. Constr.*, **2**(3), 132-137.
- Toutanji, H., Zhao, L. and Zhang, Y. (2006), "Flexural behavior of reinforced concrete beams externally strengthened with CFRP sheets bonded with an inorganic and inorganic matrix", *J. Eng. Struct.*, **28**, 557-566.